EXHIBIT A (4/4)

PNAS
Proceedings of the National Academy of Sciences of the United States of America www.pnas.org

Dilated cardiomyopathy in mice deficient for the lysosomal cysteine peptidase cathepsin L

Jörg Stypmann, Kerstin Gläser, Wera Roth, Desmond J. Tobin, Ivonne Petermann, Rainer Matthias, Gerold Mönnig, Wilhelm Haverkamp, Günter Breithardt, Wolfgang Schmahl, Christoph Peters, and Thomas Reinheckel

PNAS 2002;99;6234-6239; originally published online Apr 23, 2002;
doi:10.1073/pnas.092637699

Dilated cardiomyopathy in mice deficient for the lysosomal cysteine peptidase cathepsin L

Jörg Stypmann*†, Kerstin Gläser*‡, Wera Roth§¶, Desmond J. Tobin‖, Ivonne Petermann§, Rainer Matthias**, Gerold Mönnig†, Wilhelm Haverkamp†, Günter Breithardt†, Wolfgang Schmahl‡, Christoph Peters§††, and Thomas Reinheckel§

†Medizinische Klinik und Poliklinik C (Kardiologie und Angiologie), Zentrale Projektgruppe Kleintierdiagnostik des Interdisziplinären Zentrums für Klinische Forschung Münster, Universitätsklinikum Westfälische Wilhelms-Universität Münster, D-48149 Münster, Germany; ‡Institut für Tierpathologie, Lehrstuhl für Allegmeine Pathologie und Neuropathologie, Tierärztliche Fakultät, Ludwig-Maximilians-Universität, D-80539 Munich, Germany; §Institut für Molekulare Medizin und Zellforschung, Albert-Ludwigs-Universität Freiburg, D-79106 Freiburg, Germany; ‖Department of Biomedical Sciences, University of Bradford, Bradford, United Kingdom BD7 1DP; and **Klinik für Chirurgie, Otto-von-Guericke Universität, D-39112 Magdeburg, Germany

Edited by William S. Sly, St. Louis University School of Medicine, St. Louis, MO, and approved March 8, 2002 (received for review November 30, 2001)

Dilated cardiomyopathy is a frequent cause of heart failure and is associated with high mortality. Progressive remodeling of the myocardium leads to increased dimensions of heart chambers. The role of intracellular proteolysis in the progressive remodeling that underlies dilated cardiomyopathy has not received much attention yet. Here, we report that the lysosomal cysteine peptidase cathepsin L (CTSL) is critical for cardiac morphology and function. One-year-old CTSL-deficient mice show significant ventricular and atrial enlargement that is associated with a comparatively small increase in relative heart weight. Interstitial fibrosis and pleomorphic nuclei were found in the myocardium of the knockout mice. By electron microscopy, CTSL-deficient cardiomyocytes contained multiple large and apparently fused lysosomes characterized by storage of electron-dense heterogeneous material. Accordingly, the assessment of left ventricular function by echocardiography revealed severely impaired myocardial contraction in the CTSL-deficient mice. In addition, echocardiographic and electrocardiographic findings to some degree point to left ventricular hypertrophy that most likely represents an adaptive response to cardiac impairment. The histomorphological and functional alterations of CTSL-deficient hearts result in valve insufficiencies. Furthermore, abnormal heart rhythms, like supraventricular tachycardia, ventricular extrasystoles, and first-degree atrioventricular block, were detected in the CTSL-deficient mice.

Dilated cardiomyopathy (DCM) describes a heterogeneous group of myocardial diseases characterized by cardiac dilation, decreased contractility of the myocardium, and congestive heart failure. Among the presently known causes of DCM are enteroviral infections, ischemia, and mutations in genes encoding sarcomeric and structural proteins essential for generation and transmission of contractile forces within the cardiomyocyte. These proteins include cardiac β-myosin, troponin C, cardiac β-actin, desmin, dystrophin, δ-sarcoglycan, and the nuclear envelope protein lamin A/C (1–6). Nevertheless, the etiology of DCM remains elusive in about 50% of the patients (7). To elucidate further the pathophysiology of the disease, gain-of-function and loss-of-function mouse lines for the respective genes have been generated. Some of these lines, e.g., deletions of δ-sarcoglycan and the actin-associated muscle LIM protein MLP or a R403N point mutation in the cardiac myosin heavy chain, resemble the phenotype of human hereditary DCM (8–10). On the other hand, multiple genetically altered mouse lines developing hereditary DCM are currently lacking human counterparts, e.g., overexpression of tumor necrosis factor α or retinoic receptor α, inactivation of the cAMP response element-binding protein, and deletion of the bradikinin B2 receptor and the mitochondrial transcription factor A (Tfam; 11–17).

The lysosomal/endosomal cellular compartment is equipped with multiple glycosidases, nucleases, lipases, phosphatases, sulfatases, and peptidases for terminal degradation of macromolecules (18). Lysosomal peptidases comprise aspartic and cysteine peptidases. Most lysosomal cysteine-peptidases belong to the family of papain-like peptidases characterized by a catalytic triad, including an active-site cysteine residue (19). Seven of these papain-like lysosomal peptidases, the cathepsins B, C, F, H, L, O, and Z, are ubiquitously expressed in mammalian tissues, with myocardium among them. Other members of the family exhibit cell-type-specific expression; e.g., cathepsin S is expressed in peripheral antigen-presenting cells, but cathepsin K is mainly found in osteoclasts (20). Lysosomal cysteine peptidases are involved in unspecific bulk proteolysis in the lysosomes (21). However, evidence is growing for specific *in vivo* functions of papain-like cysteine peptidases in limited proteolysis during physiological and pathological processes such as MHC class II-mediated antigen presentation, prohormone processing, bone development, and tumor invasion (22–24). In mice, the ubiquitously expressed lysosomal cysteine peptidase cathepsin L (CTSL) is critical for epidermal homeostasis, regulation of the hair cycle, and MHC II-mediated antigen presentation in epithelial cells of the thymus (25, 26). Cardiomyopathies have been described in hereditary deficiencies of lysosomal glycosidases, like in mucopolysaccharidoses and glycogenoses (27). Furthermore, deficiency of the lysosomal membrane glycoprotein LAMP-2 has recently been shown to be the cause of Danon disease, which presents with severe cardiopathy-myopathy (28, 29).

Here we show that CTSL is essential for regular cardiac function in the mouse, because CTSL-deficient mice develop pathomorphological, histological, and functional cardiac alterations that closely resemble human DCM.

Materials and Methods

Generation and Maintenance of CTSL-Deficient Mice. CTSL-deficient mice have been generated by gene targeting in mouse embryonic stem cells as described (26). The maintenance and breeding of the animals used in this study, as well as all of the subsequent experiments including echocardiographic and electrocardiographic recordings, were performed in accordance with our institutional regulations.

This paper was submitted directly (Track II) to the PNAS office.

Abbreviations: CTSL, cathepsin L; DCM, dilated cardiomyopathy; ECM, extracellular matrix; ECG, electrocardiographic recording.

*J.S. and K.G. contributed equally to this work.

¶Present address: Genzentrum, Institut für Biochemie, Ludwig-Maximilians-Universität, D-81377 Munich, Germany.

††To whom reprint requests should be addressed. E-mail: petersc@mm11.ukl.uni-freiburg.de.

The publication costs of this article were defrayed in part by page charge payment. This article must therefore be hereby marked "*advertisement*" in accordance with 18 U.S.C. §1734 solely to indicate this fact.

www.pnas.org/cgi/doi/10.1073/pnas.092637699

Histological and Histomorphometrical Analyses. The body-to-heart weight ratio was determined by weighing the body immediately after death and the heart after removal of main vessels. After fixation in 7% unbuffered formalin and paraffin embedding, serial sections of 2-μm thickness were cut and stained with hematoxylin/eosin or Masson's trichrome. The proportion of interstitial connective tissue was determined by using the "point counting method" at 40× resolution with grid points of 18-μm distance (30). The number of cardiomyocyte nuclei per unit volume of myocardium (numeric density) was estimated by using a Physical Dissector (31, 32).

High-Resolution Light Microscopy and Transmission Electron Microscopy. Hearts were removed from 12-month-old $ctsl^{+/+}$ (n = 2) and $ctsl^{-/-}$ mice (n = 2) and immediately fixed in Karnovsky's fixative as 1-mm^3 tissue cubes. The tissues were postfixed in 2% osmium tetroxide and embedded in resin as described (33). Semithin sections were stained with toluidine blue/borax, examined by light microscopy, and photographed (Leitz). Ultrathin sections were stained with uranyl acetate and lead citrate and were examined and photographed with a Jeol ×1,200 electron microscope.

Echocardiography and Cardiac Doppler Examination. Echocardiographic examination of 40 mice was performed after intraperitoneal sedation with ketamine (50 μg/g)/xylazine (5 μg/g). Transthoracic Doppler echocardiography was performed with a digital cardiac ultrasound machine equipped with either a 12-MHz short focal-length-phased or a 15-MHz linear array transducer (SONOS 5500, B1 software package, Agilent Technologies, Andover, MA). Both parasternal long-axis and short-axis views were obtained. M-mode and Doppler recordings were performed at a sweep speed of 150 mm/s. Left ventricular septal and posterior wall thickness at the end of diastole as well as end-diastolic and end-systolic dimensions of the left ventricle were measured by using leading edge to leading edge reglementation with electronic caliper in M-mode. The percentage of fractional shortening, end-diastolic and end-systolic volume, ejection fraction, mass of left ventricle, and left ventricle mass index were calculated with conversion formulas as described (34). For determination of systolic outflow of the left ventricle, pulsed-wave Doppler signals were obtained by placing the sample volume parallel to flow during long-axis view into the left ventricular outflow tract and the ascending aorta. Diastolic inflow was detected apical to the mitral valve within the left ventricle. Both valves were examined for regurgitation with color-flow Doppler.

Electrocardiographic Recordings (ECGs). Telemetric ECGs were recorded by using a commercially available implantable transmitter and acquisition system (TA10ETA-F20-L20; DSI, St. Paul, MN), which was implanted in ketamine (50 μg/g)/xylazine (10 μg/g)-anesthetized mice according to the operative procedure described by Kramer *et al.* (35). After a recovery phase of 10 days and achievement of baseline body weight, the mice were positioned on the acquisition system. ECGs were recorded for 24 h and analyzed in LABVIEW format. Six lead-surface ECGs were recorded noninvasively (Mega-card; Siemens, Iselin, NJ) in back-spine position with tissue-covered clips with electrode gel.

Statistical Analysis. All data are reported as mean and SD. Statistical analysis was performed by using SPSS software (version 10.0; SPSS, Chicago). All data were subjected to a one-way ANOVA accounting for the four categories: wild-type ($ctsl^{+/+}$), heterozygous $ctsl^{+/-}$, CTSL-deficient mice without ($ctsl^{-/-}$) and with manifest DCM ($ctsl^{-/-}$/DCM). Whenever significant differences were detected, groups were analyzed by using Bonferroni's post hoc test. A level of $P < 0.05$ was considered to indicate significant differences between the groups.

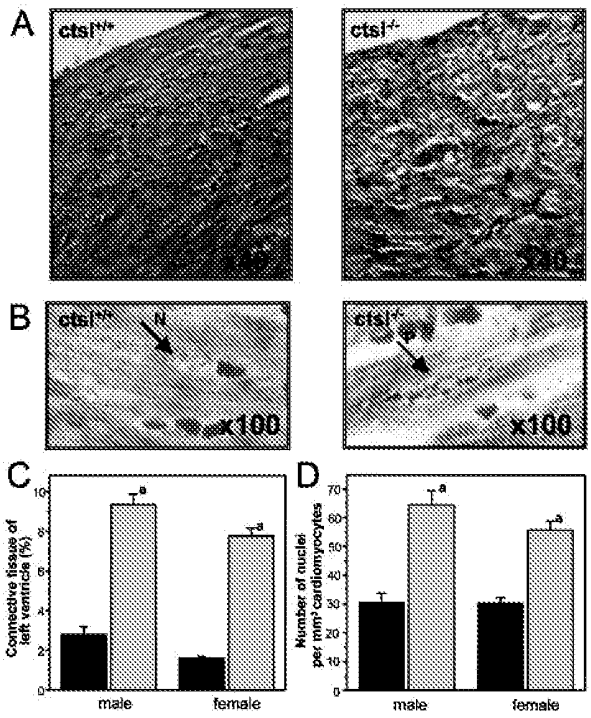

Fig. 1. Histological and histomorphometric analysis of myocardium. (*A*) Trichrome stain of myocardium of wild-type mice ($ctsl^{+/+}$) and CTSL-deficient mice ($ctsl^{-/-}$) at 12 months of age. Connective tissue appears in blue. (*B*) Large pleomorphic nucleus (P) in CTSL-deficient myocardium as compared with a normal nucleus (N). Masson's trichrome stain at 100-fold resolution. Note the distinct interstitial collagen staining in the absence of CTSL. (*C*) Histomorphometric determination of left ventricular connective tissue of wild-type (black) and CTSL-deficient (gray) mice. (*D*) Numeric density of nuclei in cardiomyocytes of wild-type (black) and CTSL-deficient (gray) ventricles. (a) $P < 0.001$ for comparison of wild-type (10 females, seven males) and knockout (nine females, five males) mice.

Results

CTSL-Deficient Mice Exhibit Altered Histology and Morphology of the Heart. CTSL-deficient mice are fertile and show normal breeding behavior. Pups devoid of CTSL exhibit a mortality rate of 15%, which is slightly higher than the 6% mortality observed for their wild-type littermates. Thereafter, mortality of both groups did not show any significant differences up to 1 year of age (26). Histological and histomorphometrical analyses of the hearts of 1-year-old mice revealed a marked increase of connective tissue in the myocardium of $ctsl^{-/-}$ mice (Fig. 1). Cardiomyocytes of $ctsl^{-/-}$ mice exhibit about twice as many nuclei per mm^3 than cardiomyocytes of control mice (Fig. 1). Consequently, the volume of cytoplasm per nucleus significantly decreased from an average of 30 μm^3 in $ctsl^{+/+}$ mice to about 15 μm^3 in $ctsl^{-/-}$ mice. In addition, many nuclei of CTSL-deficient cardiomyocytes proved to be pleomorphic, an observation that presents a general characteristic of cardiomyopathies (Fig. 1). Note that inflammatory cell infiltrates were not observed in the $ctsl^{-/-}$ hearts. For closer investigation of cellular ultrastructure, electron microscopy was performed in myocard samples of 12-month-old mice (Fig. 2). $Ctsl^{+/+}$ mice show the normal ultrastructure of heart muscle cells with rare, small, and singly scattered lysosomes. By contrast, most cells in the myocardium of age-matched $ctsl^{-/-}$ mice contain multiple large, and apparently fused, lysosomes (Fig. 2). $Ctsl^{-/-}$ lysosomes are characterized by the accumulation

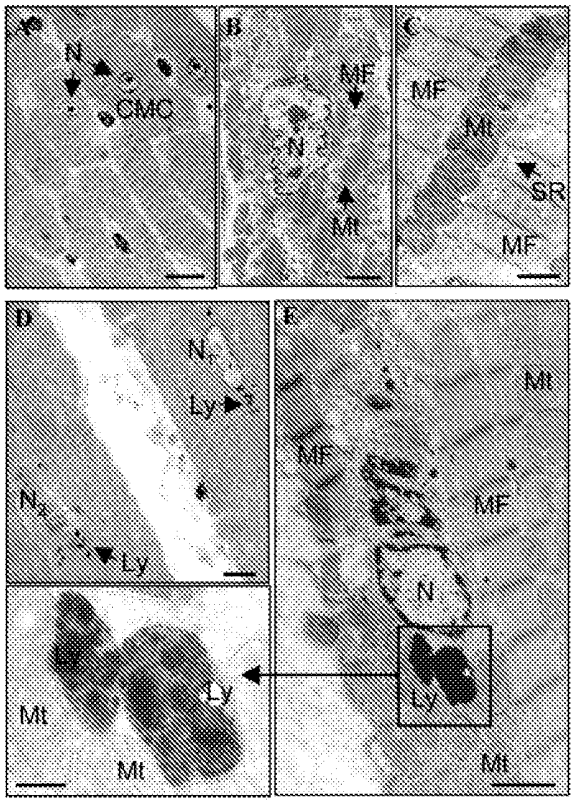

Fig. 2. Electron microscopic analysis of myocardium in 12-month-old $ctsl^{+/+}$ and $ctsl^{-/-}$ mice. (*A*) Low-power view of cardiac muscle cells (CMC) of $ctsl^{+/+}$ heart showing several typical cylindrical, striated, muscle cells (transversely cut) with a centrally located clear nucleus (N). (*B*) Medium-power view of single cardiac muscle cell with central clear nucleus (N) surrounded by numerous mitochondria (Mt) and myofibrils (MF). (*C*) High-power view of cardiac muscle cell cytoplasm showing organized arrays of myofibrils (MF) and closely packed mitochondria (MT) and sarcoplasmic reticulum. Note that lysosomes are not readily apparent in $ctsl^{+/+}$ tissue. (*D*) Low-power view of cardiac muscle cells of $ctsl^{-/-}$ heart showing two cylindrical striated muscle cells (longitudinally cut). Several lysosomes (Ly) are distributed around nuclei that may be morphologically normal (N1) or undergoing lysis (N2). (*E*) Higher-power view of a single cardiac muscle cell in $ctsl^{-/-}$ heart. Large lysosomes (Ly) are distributed close to a dystrophic nucleus (N) and surrounded by numerous mitochondria (Mt) and myofibrils (MF). (*Inset*) High-power view of lysosomes (Ly) surrounded by myofibrils (MF) and mitochondria (Mt). Lysosomes contain heterogeneous electron-dense materials. (*A* and *D*) High-resolution light microscopy, toluidine blue stain. [Scale bars: *A* and *D*, 20 μm; *B*, *C*, and *E* (transmission electron microscopy, uranyl acetate, and lead citrate), *B*, 2 μm; *C*, 1 μm; *E*, 1 μm; *Inset*, 0.3 μm.]

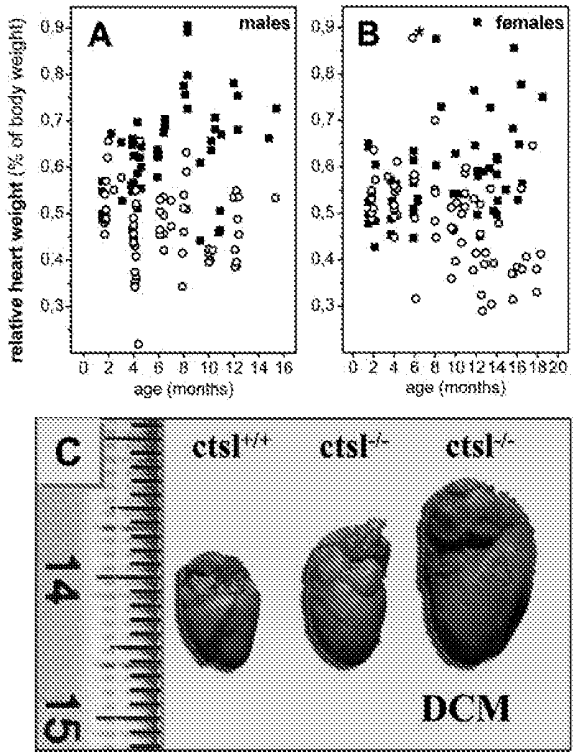

Fig. 3. Relative heart weights of CTSL-deficient mice and heart morphology. Relative heart weights of male (*A*) $ctsl^{-/-}$ (■, $n = 52$) and $ctsl^{+/+}$ (○, $n = 62$) and female (*B*) $ctsl^{-/-}$ (■, $n = 58$) and $ctsl^{+/+}$ (○, $n = 69$) mice. A 6-month-old wild-type mouse with severely enlarged heart is indicated by *. This mouse presented the only "spontaneous" heart disease seen in the 131 investigated wild-type mice. (*C*) Hearts of wild-type ($ctsl^{+/+}$) and CTSL-deficient ($ctsl^{-/-}$) mice at 12 months of age are shown. About 75% of $ctsl^{-/-}$ hearts show slight to moderate enlargement. The remaining 25% of $ctsl^{-/-}$ hearts exhibit severe enlargement with severe functional impairment, manifest DCM.

of large amounts of electron-dense heterogeneous materials and were seen most often in the perikaryon of the cell next to commonly dystrophic nuclei (Fig. 2*e*). The gross phenotype of the hearts, the amount of interstitial connective tissue (data not shown), and the relative heart weights were not altered in CTSL-deficient at 6–8 weeks of age (Fig. 3). First patches of interstitial fibrosis were observed in $ctsl^{-/-}$ hearts at 4 months (data not shown). From about 6 months of age on, the relative heart weights of CTSL-deficient mice tended to increase as compared with age-matched $ctsl^{+/+}$ controls (Fig. 3). By 12 months, hearts of all CTSL-deficient mice seemed enlarged as compared with wild-type and heterozygous mice (Fig. 3). However, about 25% of CTSL-deficient mice showed extremely enlarged hearts (Fig. 3). Because of only a moderate increase in heart weight, these mice were suspected to suffer from DCM. Hence, these findings required closer investigation of morphological and functional parameters of $ctsl^{-/-}$ hearts *in vivo*.

Dilation and Reduced Contraction of CTSL-Deficient Hearts. By means of echocardiography, a CTSL-genotype-dependent increase of left ventricular dimensions was observed in 1-year-old mice (Fig. 4). Again, four of the 14 $ctsl^{-/-}$ mice investigated by echocardiography exhibited a severe enlargement of the left ventricle with a 2- to 3-fold increase in the volumes of the left ventricle at the end of systole and diastole, which was accompanied by a 1.5-fold higher mass of the left ventricle and by enlargement of the left atrium. These observations point to the presence of DCM in this subgroup of mice (Fig. 4). However, some functional parameters of the left ventricle proved to be significantly impaired in all $ctsl^{-/-}$ hearts, which can be explained by the histopathological alterations that affect the myocardium of all CTSL-deficient mice. For example, fractional shortening, which provides a measure of left ventricular contraction, was significantly reduced in all CTSL-deficient mice, whereas the occurrence of more extreme ventricular enlargement did not further reduce contraction (Fig. 5). Accordingly, the diameter and volume of the left ventricle at maximal contraction, e.g., the end of systole, was also significantly enhanced in all $ctsl^{-/-}$ mice (Fig. 5, Table 1). The extreme dilation of hearts in about 25% of CTSL-deficient mice results in even more severe functional alterations that are unique to this subgroup of mice (Table 1). Doppler echocardiography was used for assessment of blood flow across the aortic and mitral valves (Fig. 6). By means of this technique, the maximal and average pressure gradients at the aortic valve of $ctsl^{-/-}$ mice with extremely dilated hearts were shown to be elevated 3- to 4-fold as compared with all other

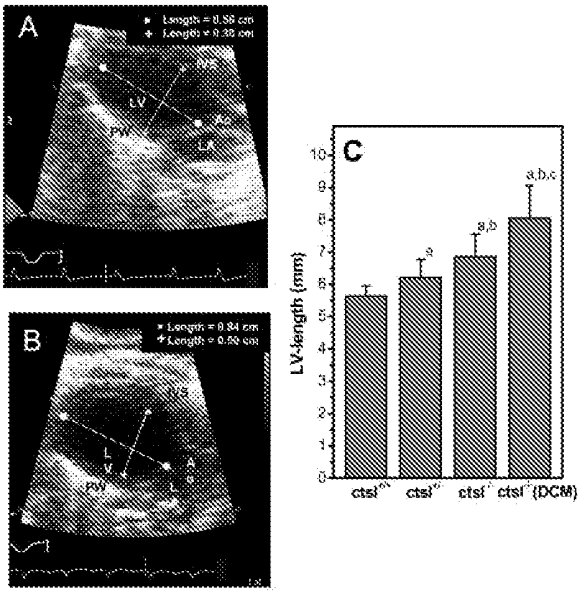

Fig. 4. *In vivo* assessment of left ventricular dimensions by echocardiography. (*A*) Two-dimensional echocardiographic picture of a normal-sized left ventricle in a 12-month-old wild-type mouse. Ao, aortic valve; LV, left ventricle; LA, left atrium; IVS, interventricular septum; PW, posterior wall. (*B*) Enlarged left ventricle of a 12-month-old CTSL-deficient mouse. (*C*) Genotype-dependent increase in the length of left ventricle. $ctsl^{+/+}$, wild-type mice; $ctsl^{+/-}$, heterozygous mice; $ctsl^{-/-}$, CTSL-deficient mice; $ctsl^{-/-}$ DCM, CTSL-deficient mice with manifest DCM. (a) $P < 0.05$ compared with $ctsl^{+/+}$, (b) $P < 0.05$ compared with $ctsl^{+/-}$, (c) $P < 0.05$ compared with $ctsl^{-/-}$.

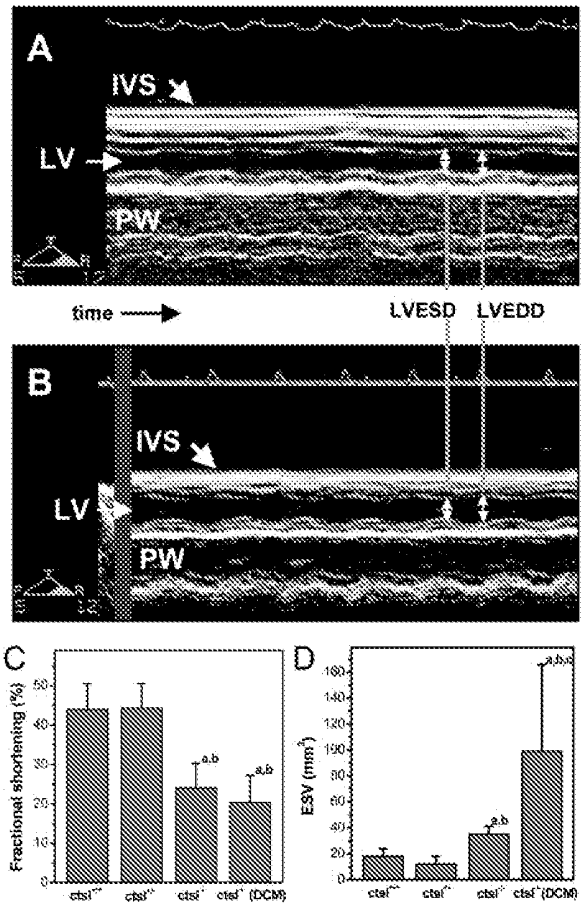

Fig. 5. Determination of heart contraction. (*A*) M-mode echocardiography showing normal contraction of the interventricular septum and the posteriolateral wall in the heart of a wild-type mouse. LV, left ventricle; IVS, interventricular septum; PW, posterior wall; LVEDD, left ventricular end-diastolic diameter; LVESD, left ventricular end-systolic diameter. (*B*) Reduced contraction of interventricular septum and posteriolateral wall in a CTSL-deficient mouse. (*C*) Fractional shortening as a measure of heart contraction and (*D*) left ventricular end-systolic volume in wild-type mice ($ctsl^{+/+}$), heterozygous mice ($ctsl^{+/-}$), CTSL-deficient mice ($ctsl^{-/-}$), and CTSL-deficient mice with manifest DCM ($ctsl^{-/-}$ DCM). (a) $P < 0.05$ compared with $ctsl^{+/+}$, (b) $P < 0.05$ compared with $ctsl^{+/-}$, (c) $P < 0.05$ compared with $ctsl^{-/-}$.

investigated groups. In addition, observation of regurgitation at the mitral and aortic valves confirmed the presence of valve insufficiencies in the dilated hearts (Fig. 6). In consequence, the cardiac index, which describes the amount of heart work needed to maintain sufficient blood perfusion of the body, is significantly increased in mice with severe ventricular and atrial dilation.

Cardiomyopathy Caused by CTSL Deficiency Is Associated with Defects in Conduction. Changes in electrophysiology of the heart assessed by ECGs are a clinical hallmark of cardiomyopathies. In contrast, alterations of heart rhythm were either not reported or not studied in many of the available mouse models for DCM. The heart rate of freely moving $ctsl^{-/-}$ and wild-type mice was similar in telemetric recording 10 days after transmitter implantation (769 vs. 755 beats per min). However, $ctsl^{-/-}$ mice presented with higher R-wave voltages in standard limb lead II (1.45 vs. 0.95 mV) as an electrocardiographic sign of left ventricular hypertrophy. Additionally, the interval between the R- and T-waves of the ECG that reports activation and repolarization time of the ventricle is prolonged in $ctsl^{-/-}$ mice (50 vs. 30 ms), especially in telemetric recording (45 vs. 22 ms), with a pathologic flat and wide T-wave morphology (data not shown). Supraventricular tachycardia was observed in three of the 14 $ctsl^{-/-}$ mice investigated. However, tachycardia was not specifically limited to the CTSL-deficient mice with manifest DCM, because one mouse with episodes of tachycardia was also detected in the group of 12 heterozygous $ctsl^{+/-}$ animals. Furthermore, one mouse with atrioventricular block and one with monomorphic ventricular extrabeats were found in the $ctsl^{-/-}$ group (data not shown).

Discussion

This article reports a critical role of the lysosomal cysteine peptidase for cardiac homeostasis in $ctsl^{-/-}$ mice. Except for a slightly increased length of the left ventricle, heterozygous mice do not show major alterations in morphology or function of the heart. A complete deficiency of CTSL in the "knockout" mice causes interstitial fibrosis in the myocardium and pleomorphic nuclei of cardiomyocytes that represent histological alterations characteristic of human cardiomyopathies. Accordingly, left ventricular contractility, assessed by echocardiographic determination of fractional shortening, was reduced in all $ctsl^{-/-}$ mice. Histological, echocardiographic and electrocardiographic findings point to the development of moderate left ventricular hypertrophy, which most likely represents an adaptive response to impaired cardiac function. In addition, pathological impairment of heart rhythm, e.g., supraventricular tachycardia, ventricular extrasystoles, and first-degree atrioventricular block, was detected in CTSL-deficient mice. However, these heterogeneous conduction defects did not occur in all $ctsl^{-/-}$ mice. Thus, it seems likely that these electrophysiological alterations are not caused by the lack of CTSL in cardiomyocytes or in the cells of the conduction system, but are rather indicative of the structural changes of the heart in the course of cardiomyopathy. Furthermore, about 25% of the hearts of $ctsl^{-/-}$ mice had developed a severe enlargement at 12 months of age, which resulted in

Table 1. Echocardiographic findings in cathepsin L-deficient mice

	ctsl$^{+/+}$ (n = 12)	ctsl$^{+/-}$ (n = 14)	ctsl$^{-/-}$ (n = 10)	ctsl$^{-/-}$ (n = 4) DCM
LVESD, mm	2.24 ± 0.35	1.90 ± 0.37	2.98 ± 0.20*†	4.44 ± 1.41*†‡
EDV, mm^3	71 ± 17	49 ± 15	68 ± 12	166 ± 105*†‡
LVEDD, mm	4.01 ± 0.44	3.41 ± 0.41	3.95 ± 0.29	5.57 ± 1.67*†‡
LV-mass, mg	88 ± 14	90 ± 17	100 ± 18	148 ± 63*†‡
LA, mm	2.12 ± 0.28	2.35 ± 0.41	2.38 ± 0.49	3.38 ± 0.94*†‡
AoV_{max}, cm/s	68.3 ± 11.0	69.9 ± 14.2	73.4 ± 19.5	116 ± 81.0*†‡
$AoPG_{max}$, mmHg	1.91 ± 0.62	2.02 ± 0.79	2.29 ± 1.29	7.36 ± 10.2*†‡
$AoPG_{mean}$, mmHg	0.97 ± 0.28	1.05 ± 0.36	1.23 ± 0.63	4.39 ± 6.47*†‡
CI, ml/min per g	0.35 ± 0.09	0.32 ± 0.69	0.46 ± 0.13	0.63 ± 0.25*†‡
AI	0	0	0	2
MI	0	0	0	2

ctsl$^{+/+}$, wild-type mice; ctsl$^{+/-}$, heterozygous mice; ctsl$^{-/-}$, cathepsin L-deficient mice; ctsl$^{-/-}$ DCM, cathepsin L-deficient mice with manifest dilated cardiomyopathy; LVESD, left ventricular end-systolic diameter; EDV, end-diastolic volume; LV-mass, calculated mass of left ventricle; LVEDD, left ventricular end-diastolic diameter; LA, diameter of left atrium; AoV_{max}, maximum velocity of flow in pw-doppler over aortic valve; $AoPG_{max}$, maximum aortic pressure gradient; $AoPG_{mean}$, average aortic pressure gradient; CI, cardiac index; AI, aortic valve insufficiency; MI, mitralic valve insufficiency.

*Statistical significance by Wilcoxon rank sum test: $P < 0.05$ compared with ctsl$^{+/+}$.

†Statistical significance by Wilcoxon rank sum test: $P < 0.05$ compared with ctsl$^{+/-}$.

‡Statistical significance by Wilcoxon rank sum test: $P < 0.05$ compared with ctsl$^{-/-}$.

significantly impaired cardiac performance and led to valve insufficiencies in four of the 14 CTSL-deficient mice investigated by Doppler echocardiography. Despite these histomorphological and functional alterations, the mortality rate of adult *ctsl*$^{-/-}$ mice was not increased in mice up to 12 months of age, which contrasts with many other transgenic mouse models of DCM in which symptoms occur early in life and result in death only days or a few weeks after onset of the disease (9, 10, 14, 16, 17, 36). Thus, CTSL-deficient mice represent a model of a chronic progressive DCM that is comparable to the adult form of the human disease in many respects. This model could greatly serve the study of effects of additional exercise on morphology and function of the heart and the long-term assessment of novel treatment options.

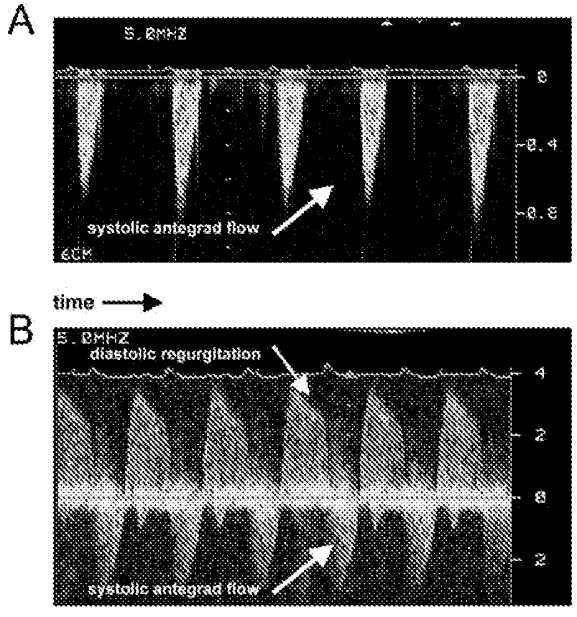

Fig. 6. Functional assessment of heart valves by pulse-waved Doppler-echocardiography. (*A*) Wild-type mouse showing normal antegrade flow through the aortic valve. (*B*) Aortic regurgitation and high velocity of aortic antegrade flow as hallmarks of aortic valve insufficiency in a *ctsl*$^{-/-}$ mouse.

To date, multiple genetic loci affected in familiar DCM have been identified. However, the disease-causing gene is often not known yet (37). Most notably, the gene encoding human CTSL is located at chromosome 9q21-q22, which corresponds to the genetic mapping of a familiar DCM trait with an unidentified disease-causing gene at chromosome 9q13-q22 (38). Thus, in combination with the present findings in *ctsl*$^{-/-}$ mice, CTSL is a potential DCM-causing gene in humans.

Most notably, a complete deficiency of CTSL in mice causes accumulation of heterogeneous electron-dense material in significantly enlarged lysosomes, which is clearly indicative for lysosomal storage that would place the heart phenotype of CTSL-deficient mice in a group of lysosomal metabolic cardiomypopathies, such as the deficiency of the lysosomal membrane protein Lamp-2 (Danon disease) or constitutively activating AMP kinase mutations that cause lysosomal glycogen storage (28, 29, 39). However, although the latter disorders show impaired cardiac function, they are not characterized by ventricular dilation. Thus, the pathogenesis of the heart dilation caused by CTSL deficiency still needs to be elucidated. Currently, the leading hypothesis regarding the pathogenesis of DCM is focused on alterations in production of contractile force in the sarcomere and/or impaired force transmission to the plasma membrane of cardiomyocytes (37). Although electron microscopy revealed intact cardiac sarcomeres of *ctsl*$^{-/-}$ mice, multiple possibilities remain how CTSL maintains the contractile function of cardiomyocytes. First, lysosomal cysteine peptidases, among them CTSL, are responsible for up to 40% of intracellular protein turnover (40, 41). Many proteins of the cytoskeleton with relatively long biological half-life are considered to be subject to lysosomal degradation. Thus, partial impairment of lysosomal proteolysis by the constitutive absence of CTSL may lead to an altered balance between synthesis and degradation of cytoskeletal proteins. This altered balance could result in a functional disturbance of the contractile apparatus and in subsequent cardiac remodeling that eventually progresses into maladaptive DCM in some of the *ctsl*$^{-/-}$ mice. Second, lysosomal cysteine peptidases of the papain family exhibit high collagenolytic and elastinolytic activity. In fact, the plant protease papain is a common meat tenderizer (23). Although CTSL is located mainly in the endosomal/lysosomal compartment, about 10% of the zymogen is physiologically secreted and can be extracellularly activated (42). There, it is capable of processing

extracellular matrix (ECM) proteins such as fibronectin, laminin, and types I, IV, and XVIII collagen (42, 43). For example, CTSL can cleave within the nonhelical regions at the ends of native collagen, which leads to destabilization of the fibrils and promotes further cleavage by other proteases like matrix metalloproteinases (43). Extracellular CTSL is also able to activate other proteases such as urokinase-type plasminogen activators (44). Hence, the absence of CTSL could lead to gradually increasing interstitial fibrosis caused by defective degradation of proteins in the ECM. Because the ECM provides the "anchor" for the contractile forces produced by the sarcomere, changes in composition and organization of ECM could result in impaired force transmission and, therefore, cardiac dilation or hypertrophy. This possibility is supported by recent findings that matrix metalloproteinases, which function primarily in degradation of ECM, are critically involved in the development of heart failure in several mouse models (45).

In summary, a function for the lysosomal peptidase CTSL has been found in the maintenance of heart structure and function. Absence of CTSL results in lysosomal impairment that causes the development of a heart disease that resembles many features of human DCM. CTSL is a candidate gene for the human hereditary DCM mapped to chromosome 9q13-q22. To date, the molecular mechanisms by which CTSL serves its essential function in the heart remain elusive, but nevertheless, CTSL-deficient mice could serve as a DCM model for the study of challenge phenotypes and treatment options.

C.P. dedicates this work to Friedhelm Beyersdorf (Freiburg). This work was supported by the Deutsche Forschungsgemeinschaft SFB 556 (Teilprojekt Z2; to W.H.) and the Fonds der Chemischen Industrie (to C.P.).

1. Kamisago, M., Sharma, S. D., DePalma, S. R., Solomon, S., Sharma, P., McDonough, B., Smoot, L., Mullen, M. P., Woolf, P. K., Wigle, E. D., *et al.* (2000) *N. Engl. J. Med.* **343,** 1688–1696.
2. Olson, T. M., Michels, V. V., Thibodeau, S. N., Tai, Y. S. & Keating, M. T. (1998) *Science* **280,** 750–752.
3. Li, D., Tapscoft, T., Gonzalez, O., Burch, P. E., Quinones, M. A., Zoghbi, W. A., Hill, R., Bachinski, L. L., Mann, D. L. & Roberts, R. (1999) *Circulation* **100,** 461–464.
4. Towbin, J. A., Hejtmancik, J. F., Brink, P., Gelb, B., Zhu, X. M., Chamberlain, J. S., McCabe, E. R. & Swift, M. (1993) *Circulation* **87,** 1854–1865.
5. Tsubata, S., Bowles, K. R., Vatta, M., Zintz, C., Titus, J., Muhonen, L., Bowles, N. E. & Towbin, J. A. (2000) *J. Clin. Invest.* **106,** 655–662.
6. Brodsky, G. L., Muntoni, F., Miocic, S., Sinagra, G., Sewry, C. & Mestroni, L. (2000) *Circulation* **101,** 473–476.
7. Follath, F. (1999) *J. Cardiovasc. Pharmacol.* **33,** Suppl. 3, S31–S35.
8. Coral-Vazquez, R., Cohn, R. D., Moore, S. A., Hill, J. A., Weiss, R. M., Davisson, R. L., Straub, V., Barresi, R., Bansal, D., Hrstka, R. F., *et al.* (1999) *Cell* **98,** 465–474.
9. Arber, S., Hunter, J. J., Ross, J., Hongo, M., Sansig, G., Borg, J., Perriard, J. C., Chien, K. R. & Caroni, P. (1997) *Cell* **88,** 393–403.
10. Fatkin, D., Christe, M. E., Aristizabal, O., McConnell, B. K., Srinivasan, S., Schoen, F. J., Seidman, C. E., Turnbull, D. H. & Seidman, J. G. (1999) *J. Clin. Invest.* **103,** 147–153.
11. Bryant, D., Becker, L., Richardson, J., Shelton, J., Franco, F., Peshock, R., Thompson, M. & Giroir, B. (1998) *Circulation* **97,** 1375–1381.
12. Kubota, T., McTiernan, C. F., Frye, C. S., Slawson, S. E., Lemster, B. H., Koretsky, A. P., Demetris, A. J. & Feldman, A. M. (1997) *Circ. Res.* **81,** 627–635.
13. Colbert, M. C., Hall, D. G., Kimball, T. R., Witt, S. A., Lorenz, J. N., Kirby, M. L., Hewett, T. E., Klevitsky, R. & Robbins, J. (1997) *J. Clin. Invest.* **100,** 1958–1968.
14. Fentzke, R. C., Korcarz, C. E., Lang, R. M., Lin, H. & Leiden, J. M. (1998) *J. Clin. Invest.* **101,** 2415–2426.
15. Emanueli, C., Maestri, R., Corradi, D., Marchione, R., Minasi, A., Tozzi, M. G., Salis, M. B., Straino, S., Capogrossi, M. C., Olivetti, G. & Madeddu, P. (1999) *Circulation* **100,** 2359–2365.
16. Li, H., Wang, J., Wilhelmsson, H., Hansson, A., Thoren, P., Duffy, J., Rustin, P. & Larsson, N. G. (2000) *Proc. Natl. Acad. Sci. USA* **97,** 3467–3472.
17. Wang, J., Wilhelmsson, H., Graff, C., Li, H., Oldfors, A., Rustin, P., Bruning, J. C., Kahn, C. R., Clayton, D. A., Barsh, G. S., *et al.* (1999) *Nat. Genet.* **21,** 133–137.
18. Kornfeld, S. & Mellman, I. (1989) *Annu. Rev. Cell Biol.* **5,** 483–525.
19. Rawlings, N. D. & Barrett, A. J. (2000) *Nucleic Acids Res.* **28,** 323–325.
20. Turk, B., Turk, D. & Turk, V. (2000) *Biochim. Biophys. Acta* **1477,** 98–111.
21. Barrett, A. J. (1992) *Ann. N. Y. Acad. Sci.* **674,** 1–15.
22. Villadangos, J. A., Bryant, R. A., Deussing, J., Driessen, C., Lennon-Dumenil, A. M., Riese, R. J., Roth, W., Saftig, P., Shi, G. P., Chapman, H. A., *et al.* (1999) *Immunol. Rev.* **172,** 109–120.
23. Chapman, H. A., Riese, R. J. & Shi, G. P. (1997) *Annu. Rev. Physiol.* **59,** 63–88.
24. Kirschke, H., Eerola, R., Hopsu-Havu, V. K., Bromme, D. & Vuorio, E. (2000) *Eur. J. Cancer* **36,** 787–795.
25. Nakagawa, T., Roth, W., Wong, P., Nelson, A., Farr, A., Deussing, J., Villadangos, J. A., Ploegh, H., Peters, C. & Rudensky, A. Y. (1998) *Science* **280,** 450–453.
26. Roth, W., Deussing, J., Botchkarev, V. A., Pauly-Evers, M., Saftig, P., Hafner, A., Schmidt, P., Schmahl, W., Scherer, J., Anton-Lamprecht, I., Von Figura, K., Paus, R. & Peters, C. (2000) *FASEB J.* **14,** 2075–2086.
27. Guertl, B., Noehammer, C. & Hoefler, G. (2000) *Int. J. Exp. Pathol.* **81,** 349–372.
28. Tanaka, Y., Guhde, G., Suter, A., Eskelinen, E. L., Hartmann, D., Lullmann-Rauch, R., Janssen, P. M., Blanz, J., von Figura, K. & Saftig, P. (2000) *Nature (London)* **406,** 902–906.
29. Nishino, I., Fu, J., Tanji, K., Yamada, T., Shimojo, S., Koori, T., Mora, M., Riggs, J. E., Oh, S. J., Koga, Y., *et al.* (2000) *Nature (London)* **406,** 906–910.
30. Cruz-Orive, L. M. & Weibel, E. R. (1990) *Am. J. Physiol.* **258,** L148–L156.
31. Gundersen, H. J. (1986) *J. Microsc. (Oxford)* **143,** 3–45.
32. Gundersen, H. J. & Jensen, E. B. (1987) *J. Microsc. (Oxford)* **147,** 229–263.
33. Tobin, D. J., Fenton, D. A. & Kendall, M. D. (1991) *Am. J. Dermatopathol.* **13,** 248–256.
34. Collins, K. A., Korcarz, C. E., Shroff, S. G., Bednarz, J. E., Fentzke, R. C., Lin, H., Leiden, J. M. & Lang, R. M. (2001) *Am. J. Physiol.* **280,** H1954–H1962.
35. Kramer, K., van Acker, S. A., Voss, H. P., Grimbergen, J. A., van der Vijgh, W. J. & Bast, A. (1993) *J. Pharmacol. Toxicol. Methods* **30,** 209–215.
36. Sussman, M. A., Welch, S., Cambon, N., Klevitsky, R., Hewett, T. E., Price, R., Witt, S. A. & Kimball, T. R. (1998) *J. Clin. Invest.* **101,** 51–61.
37. Seidman, J. G. & Seidman, C. (2001) *Cell* **104,** 557–567.
38. Krajinovic, M., Pinamonti, B., Sinagra, G., Vatta, M., Severini, G. M., Milasin, J., Falaschi, A., Camerini, F., Giacca, M. & Mestroni, L. (1995) *Am. J. Hum. Genet.* **57,** 846–852.
39. Arad, M., Benson, D. W., Perez-Atayde, A. R., McKenna, W. J., Sparks, E. A., Kanter, R. J., McGarry, K., Seidman, J. G. & Seidman, C. E. (2002) *J. Clin. Invest.* **109,** 357–362.
40. Shaw, E. & Dean, R. T. (1980) *Biochem. J.* **186,** 385–390.
41. Knop, M., Schiffer, H. H., Rupp, S. & Wolf, D. H. (1993) *Curr. Opin. Cell Biol.* **5,** 990–996.
42. Felbor, U., Dreier, L., Bryant, R. A., Ploegh, H. L., Olsen, B. R. & Mothes, W. (2000) *EMBO J.* **19,** 1187–1194.
43. Maciewicz, R. A. & Etherington, D. J. (1988) *Biochem. J.* **256,** 433–440.
44. Lah, T. T. & Kos, J. (1998) *Biol. Chem.* **379,** 125–130.
45. Lee, R. T. & Libby, P. (2000) *J. Clin. Invest.* **106,** 827–828.